# A New High-Pressure Polar Phase of Crystalline Bromoform: A First-Principles Study

**Gang Bao,[†,‡] Defang Duan,[†] Dawei Zhou,[†] Xilian Jin,[†] Bingbing Liu,[†] and Tian Cui*[,†]**

*State Key Lab of Superhard Materials, College of Physics, Jilin University, Changchun 130012, People's Republic of China, College of Physics and Electronic Information, Inner Mongolia University for the Nationalities, Tongliao 028043, People's Republic of China*

*Received: April 27, 2010; Revised Manuscript Received: September 23, 2010*

The high-pressure phases of bromoform at zero temperature have been investigated by first-principles pseudopotential plane-wave calculations based on the density functional theory. A new high-pressure polar phase, $\varepsilon$, with space group *CC* has been found after a series of simulated annealing and geometry optimizations. Our calculated enthalpies showed that the transition from $\beta$ phase to $\gamma$ phase occurs at 1 GPa, then the $\gamma$ phase transforms to the $\varepsilon$ phase at 90 GPa. In addition, the Br···Br and C−H···Br interactions are the key factors for the polar aggregation in the $\varepsilon$ phase. Further calculations show that the insulate−metal transition in $\varepsilon$ phase due to band overlap happens at ∼130 GPa.

## Introduction

Polar molecules of organic matter are of particular interest in chemistry, physics, and materials science.[1] The presence of polar molecules in crystals is an essential requirement for materials to have technological and industrial applications for nonlinear optics; optoelectronic transducers; ferro-, piezo-, and pyroelectric materials; actuators; and other applications.[2] High pressure is ideally suited to the study of methane,[3,4] halogens,[5−7] and halogen-substituted methanes[8,9] because the application of pressure can cause considerable variations in electronic structure, weak interactions, and significant reorganizations of crystal packing. It is found that methane decomposes to form hydrogen and diamond at 25 GPa and 7300 K. For halogens, pressure-induced insulator−metal transition proceeds in the molecular phase, and further compression forces their molecular bonding to break up and to stabilize a monatomic crystal form. Haloforms belong to the simplest halogen-substituted methanes, which are made up of molecular units of the type $CHX_3$ where X = F, C1, Br, or I. Chloroform ($CHCl_3$) and bromoform ($CHBr_3$), which are nonpolar phase at ambient conditions, can form polar phases under high pressure. As the case of iodoform ($CHI_3$), a discontinuous frequency shift is related to the enhancement of the C−H···I weak hydrogen bonds under high pressures. Bromoform, as a liquid of relatively high density, is used for mineral ore separation in geological tests. It has also been used as a sedative, anesthetic, and a cough suppression agent. In this paper, a novel high-pressure phase with polar symmetry and metallic properties for bromoform is found based on first-principles calculations, which maybe have more wildly technological applications.

At ambient pressure, the studies on the temperature dependence of bromoform ($CHBr_3$) by neutron powder diffraction revealed three different crystalline phases, denoted as the α, $\beta$, and $\gamma$ phases.[10] The crystal structures of these phases are presented in Figure 1. The α phase exists in the span from 281 to 268 K, which is dynamically disordered with their principal axes randomly parallel or antiparallel to each other. The average symmetry is represented by the space group $P6_3/m$, with four molecules per unit cell. The $\beta$ phase could be obtained by slowly cooling from the disordered α phase, observed between 268 and 14 K. The structure of $\beta$ phase is centrosymmetric triclinic with space group $P\bar{1}$, and contains two antiparallel molecules in the unit cell. The $\gamma$ phase was formed by rapidly cooling the liquid or the α phase to liquid nitrogen temperatures. The structure is now described by a centrosymmetric trigonal Bravais lattice with space group $P\bar{3}$ and contains two antiparallel molecules in the unit cell. On the other hand, the $\gamma$ phase transforms irreversibly into the $\beta$ phase by annealing above 200 K; thereby, it is commonly considered that the $\beta$ phase is stable and the $\gamma$ phase is metastable at ambient pressure.

High-pressure phase transitions at room temperature have been investigated for bromoform by Raman scatter experiment. The α phase transforms to the $\beta$ phase at 1.0 GPa[11] or 0.8 GPa[12] and further transitions into the $\gamma$ phase at 4.2 GPa[11] or 5.15 GPa.[12] It is also noticed that the $\beta$ and $\gamma$ phases coexist over an extended pressure range from 3.3 to 5.5 GPa, and the $\gamma$ phase is metastable at atmospheric pressure but becomes stable above 4.2 GPa. Recently, a new high-pressure phase $\delta$-$CHBr_3$ with polar symmetry (space group $P6_3$) was observed[13] between 0.20 and 0.35 GPa by single-crystal X-ray diffraction at 295 K.

Several theoretical works on bromoform have been performed. The orientational disorder in the α phase was postulated by a statistical model.[14] Later, the α, $\beta$, and $\gamma$ phases of bromoform were systematically studied by group theory,[15] and a phase diagram was obtained by minimizing their free energies. In addition, a description for the different phase transitions in crystalline bromoform at ambient pressure is proposed using simple intermolecular potentials.[16] Up to now, the theoretical attempts were made only to elucidate the character of disorder phase and phase transitions at ambient pressure. However, there is no investigation of solid bromoform under higher pressures by means of first principles based on density functional theory (DFT).

Most of the experimental studies on bromoform have been concentrated on vibration spectra and investigations of phase transition under high pressure, which were all carried out below 10.2 GPa.[11,12,17] They were carried out over a limited pressure range. We have studied the high-pressure behavior of bromoform up to 300 GPa at $T = 0$ K by means of first-principles

* Corresponding author. E-mail: cuitian@jlu.edu.cn.
† Jilin University.
‡ Inner Mongolia University for the Nationalities.

10.1021/jp103823c 
Published on Web 10/15/2010

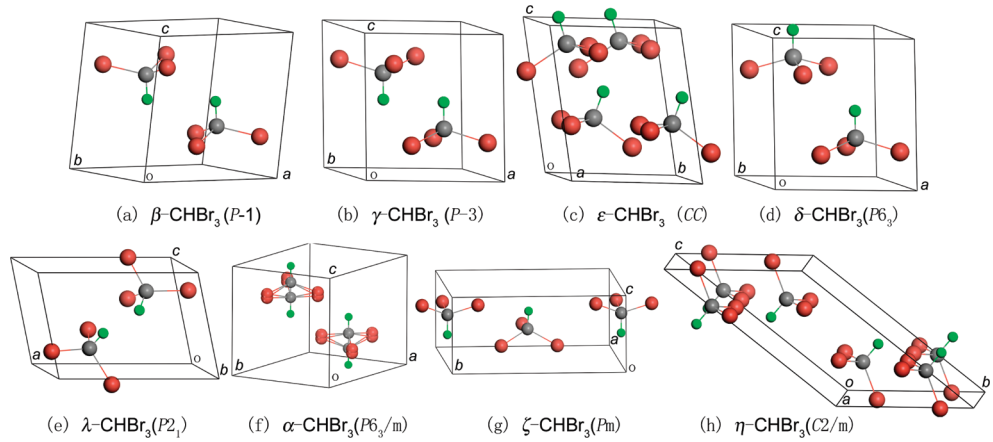


**Figure 1.** The crystal structures of solid bromoform: (a) $\beta$-$CHBr_3$, (b) $\gamma$-$CHBr_3$, (c) α-$CHBr_3$, (d) $\delta$-$CHBr_3$, (e) $\varepsilon$-$CHBr_3$, (f) $\lambda$-$CHBr_3$, (g) $\zeta$-$CHBr_3$, and (h) $\eta$-$CHBr_3$. The brown, gray, and green spheres represent bromine, carbon, and hydrogen atoms, respectively.

DFT methods. Studies of bromoform under high pressure can not only shed light on the nature of hydrogen and halogen bonds but also assist in the investigation of phase transitions, polymorphism, and molecular aggregation. Therefore, a high-pressure study for the understanding of the structural stability of bromoform is of fundamental importance.

## Methodology

The structure optimization and electronic properties were calculated by means of the pseudopotential plane-wave method within the DFT implemented in the CASTEP code.[18] All the structure optimizations under high pressure in this paper, including the atomic positions and the lattice constants, were performed by the Broyden−Fletcher−Goldfarb−Shanno algorithm.[20] The optimization was not finished until the forces on the atoms were less than 0.01 eV/Å and all the stress components were less than 0.02 GPa. The tolerance in the self-consistent field calculation was $5 \times 10^{-7}$ eV/atom. We used ultrasoft pseudopotentials[19] for H, C, and Br with electronic configuration of 1s, $2s^2 2p^2$, and $4s^2 4p^5$, respectively.

The core radius was chosen as 0.8 au for s orbitals for H; 1.4 au for s and p orbitals for C; and 2.0 and 1.9 au for s and p orbitals for Br, respectively, to guarantee the nonexistence of core overlapping under highest pressure in this study. The generalized gradient approximation in the scheme of Perdew−Burke−Eruzerhof[21] was used to describe the exchange and correlation potential. To confirm the convergence of our calculations, we carefully investigated the dependences of the total energy on the cutoff energy and the Monkhorst−Pack[22] grid.

Convergence tests gave a kinetic energy cutoff $E_{cutoff}$ as 460 eV and Brillouin zone sampling using a grid of spacing $2\pi \times 0.04$ Å$^{-1}$ for all phases. The electronic structures were calculated with higher level of accuracy using a Brillouin zone sampling of $2\pi \times 0.02$ Å$^{-1}$. Density of states (DOS) calculation was based on the Gaussian smearing of the energy levels of each band with a width of 0.2 eV. Partial density of states (PDOS) calculation is based on Mulliken population analysis, which allows you to calculate the contribution from each energy band to a given atomic orbital. Phonons were calculated by means of the direct method implemented in PHONON code,[23] and the Hellmann−Feynman forces were obtained by CASTEP code. The classical simulated annealing for crystal structure prediction has been done with the Forcite module of the Materials Studio software package.[24] We chose the COMPASS force field and used the Ewald summation method to calculate the electrostatic interactions and van der Waals interactions. Initial and midcycle temperatures were chosen to be 300 and 500 K, and 10 cycles were computed with 10 heating ramps per cycle and 100 dynamics steps per ramp. At each temperature step, the dynamics calculations were performed to ensure the structural relaxation. The NVT ensemble was adopted with a time step of 1.0 fs and a Nose thermostat with $Q$ ratio of 1.0. The phonon frequencies at Γ point were carried out using linear response theory through the Quantum-ESPRESSO package.[25]

## Results and Discussion

Because the high-pressure structures of bromoform are unknown, we take the structures $\beta$ and $\gamma$ as starting points, perform a series of simulated annealing and geometry optimization, and obtain four structures with different symmetries. They are monoclinic Bravais lattices with $CC$ (denoted as the $\varepsilon$ phase), $P2_1$ (denoted as the $\lambda$ phase), $Pm$ (denoted as the $\zeta$ phase), and $C2/m$ (denoted as the $\eta$ phase) symmetries, as shown in Figure 1.

It is used to discuss the stability of a structure from three aspects: thermodynamic, dynamical, and mechanical. The enthalpies difference of the three known ordered phases ($\beta$-$CHBr_3$, $\gamma$-$CHBr_3$, $\delta$-$CHBr_3$) and the four new phases ($\varepsilon$-$CHBr_3$, $\lambda$-$CHBr_3$, $\zeta$-$CHBr_3$, and $\eta$-$CHBr_3$) with respect to $\gamma$-$CHBr_3$ are presented in Figure 2. At ambient pressure, the $\beta$ phase is the most stable one, but the $\gamma$ phase is favored above 1 GPa, which has the lowest enthalpy in the pressure range from 1 to 90 GPa. The monoclinic $\varepsilon$ phase has the lowest enthalpy compared with all other phases in the pressure range from 90 GPa to at least 300 GPa, which is the highest pressure we calculated, suggesting that the $\varepsilon$ phase becomes the most stable one thermodynamically. The previous experiment[11] showed that the $\beta$ phase transformed to the $\gamma$ phase at 4.2 GPa, which was stable up to 10.2 GPa at room temperature, which was the largest pressure measured. Our DFT calculations correctly describe the order from the $\beta$ to $\gamma$ phase transition observed experimentally, but with a different transition pressure. However, the experiments were carried out at room temperature, whereas the calculations are performed at $T = 0$ K. In general, the temperature is less effective than pressure in producing solid−solid phase transitions, which only leads to hysteresis in the transformation. The entropy contribution does not affect the phase transition order, but slightly changes the transition pressures between different phases.[26,27] Thus, the difference of transition pressure maybe mainly attributed to a temperature effect. The $\delta$, $\lambda$, $\zeta$, and $\eta$ phases have higher enthalpies in the pressure range from 0 to

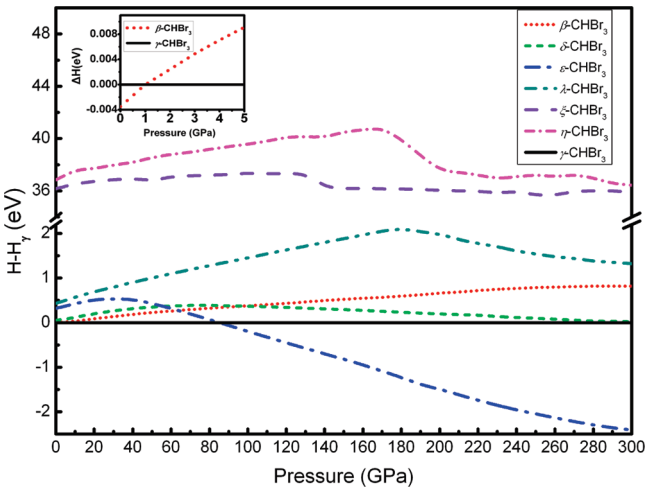


**Figure 2.** Calculated enthalpy differences for seven structures of bromoform (relative to $\gamma$ phase) as functions of pressure. Inset: the magnified enthalpy differences of $\beta$ phase compared with the $\gamma$ phase.

**TABLE 1: The Calculated Phonon Frequencies of the $\beta$ Phase in Solid $CHBr_3$ Compared with Experimental Data at 0 GPa and 0 K**

| mode ($A_g$) | our work (0 K) ($cm^{-1}$) | exptl[28] (20 K) ($cm^{-1}$) | exptl[29] (98 K) ($cm^{-1}$) |
|---|---|---|---|
| asymmetric C−Br bend | 148.91 | 156.0 | 158.5 |
| | 149.9 | 157.0 | |
| symmetric C−Br bend | 219.7 | 221.5 | 223.0 |
| symmetric C−Br stretch | 527.8 | 536.5 | 538.5 |
| asymmetric C−Br stretch | 636.7 | 654.5 | 654.5 |
| | 637.05 | 657.0 | 657.0 |
| C−H bend | 1137.8 | 1142.5 | 1144.0 |
| | 1139.3 | 1145.5 | 1146.5 |
| C−H stretch | 2984.5 | 3026.4 | 3025.5 |
| lattice | 31.2 | 30.0 | 30.5 |
| | 34.5 | 33.5 | 33.0 |
| | 41.3 | 38.5 | 37.5 |
| | 46.5 | 48.5 | 47.0 |
| | 56.5 | 52.5 | 51.5 |
| | 148.9 | 68.5 | 64.0 |

300 GPa, suggesting that these structures are unstable thermodynamically at 0 K.

A well-known dynamical instability of one structure is associated with a soft phonon with imaginary frequency. To investigate the stability of the new high pressure structure, we calculated the phonon frequencies of $\varepsilon$ phase at 100, 200, and 300 GPa in the whole Brillouin zone presented in Figure 3. The absence of imaginary frequency modes in phonon dispersion curves indicates that the $\varepsilon$ phase is dynamically stable in the pressure range from 100 to 300 GPa. In addition, the strongest C−H stretching vibrations of the $\varepsilon$ phase observed around 110 THz in a high-energy region exhibit obvious molecular feature. We also investigate the phonon frequencies of the $\beta$ phase at the Γ point, the results listed in Table 1. Our results show that the intramolecular vibration modes are in agreement with the experimental data quantitatively, and the intermolecular vibration modes agree with the experimental data to some extent.

The mechanical stability of the crystal requires the strain energy to be positive, which implies that the whole set of elastic constant $C_{ij}$ satisfies the Born stability criterion.[30] For the monoclinic crystal, the independent elastic stiffness tensor reduces to 13 components—$C_{11}$, $C_{22}$, $C_{33}$, $C_{44}$, $C_{55}$, $C_{66}$, $C_{12}$, $C_{13}$, $C_{15}$, $C_{23}$, $C_{25}$, $C_{35}$, and $C_{46}$—in the Voigt notation. The Born stability criteria for monoclinic system is given by

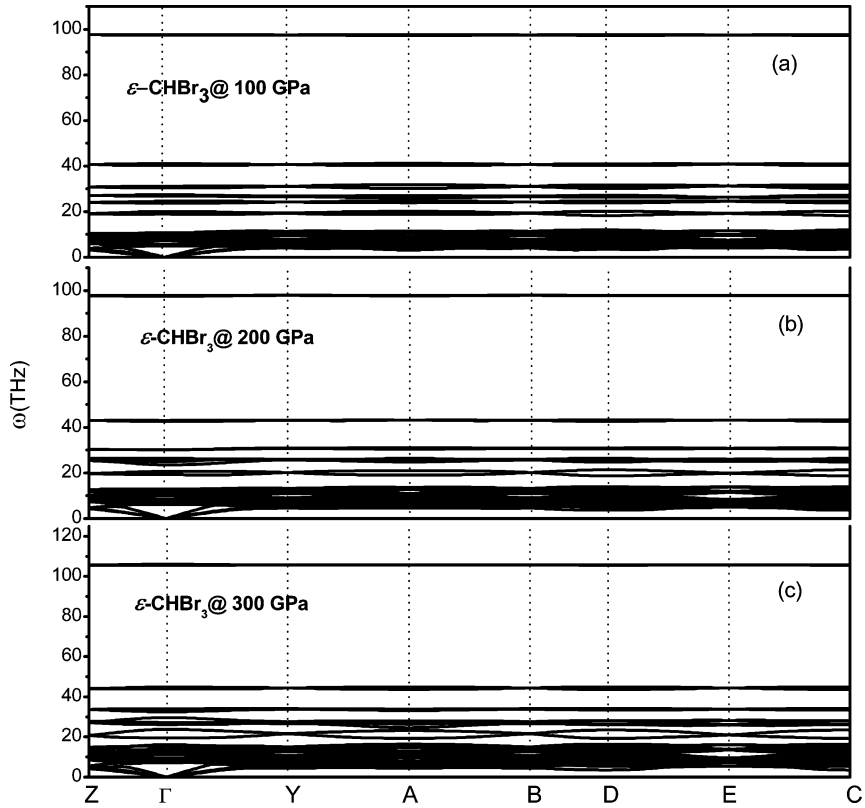


**Figure 3.** Calculated phonon dispersion curve of the $\varepsilon$ phase at pressures of 100, 200, and 300 GPa.

**TABLE 2: The Calculated Elastic Constants (in GPa) of the ε Phase at 100, 200, and 300 GPa**

| $P$ (GPa) | $C_{11}$ | $C_{22}$ | $C_{33}$ | $C_{44}$ | $C_{55}$ | $C_{66}$ | $C_{12}$ | $C_{13}$ | $C_{15}$ | $C_{23}$ | $C_{25}$ | $C_{35}$ | $C_{46}$ |
|---|---|---|---|---|---|---|---|---|---|---|---|---|---|
| 100 | 679 | 645 | 753 | 120 | 206 | 191 | 274 | 24.1 | 17.4 | 222 | 11.5 | −7.09 | 95.8 |
| 200 | 1128 | 985 | 1133 | 359 | 323 | 353 | 436 | 591 | 38.5 | 490 | 38.5 | 38.5 | 20.2 |
| 300 | 1541 | 1453 | 1531 | 521 | 359 | 530 | 651 | 879 | 29.5 | 743 | 44.9 | 2.03 | −44.8 |

$$
\begin{aligned}
&C_{ii} > 0, (i = 1, ..., 6)\\
&[C_{11} + C_{22} + C_{33} + 2(C_{12} + C_{13} + C_{23})] > 0,\\
&(C_{33}C_{55} - C_{35}^2) > 0, (C_{44}C_{66} - C_{46}^2) > 0,\\
&(C_{22} + C_{33} - 2C_{23}) > 0,\\
&[C_{22}(C_{33}C_{55} - C_{35}^2) + 2C_{23}C_{25}C_{35} - C_{23}^2C_{55} - C_{25}^2C_{33}) > 0,\\
&\{2[C_{15}C_{25}(C_{33}C_{12} - C_{13}C_{23}) + C_{15}C_{35}(C_{22}C_{13} - C_{12}C_{23}) +\\
&C_{25}C_{35}(C_{11}C_{23} - C_{12}C_{13})] - [C_{15}^2(C_{22}C_{33} - C_{23}^2C_{11}) +\\
&C_{25}^2(C_{11}C_{33} - C_{13}^2) + C_{35}^2(C_{11}C_{22} - C_{12}^2)] + C_{55}g\} > 0,\\
&(g = C_{11}C_{22}C_{33} - C_{11}C_{23}^2 - C_{22}C_{13}^2 - C_{33}C_{12}^2 + 2C_{12}C_{12}C_{23})
\end{aligned}
\tag{1}
$$

The elastic constants of ε phase calculated at 100, 200, and 300 GPa are listed in Table 2. All of the elastic constants satisfy the Born stability criteria, suggesting that this structure is mechanical stability from 100 to 300 GPa.

It is reported that the δ phase naturally polar symmetry is observed at room temperature and 0.2−0.35 GPa.[13] The calculated phonon dispersion curves of δ phase at 5 GPa is plotted in Figure 4. No imaginary phonon frequencies are found, proving that this structure is dynamically stable. Furthermore, we calculated the elastic constants of the δ phase: $C_{11} = 51.94$ GPa, $C_{33} = 37.25$ GPa, $C_{44} = 11.1$ GPa, $C_{12} = 18.96$ GPa, and $C_{13} = 28.86$ GPa, which satisfy the Born stability criteria for a hexagonal crystal,[28] $C_{44} > 0$, $C_{11} > |C_{12}|$, $(C_{11} + 2C_{12})C_{33} > 2C_{13}^2$, indicating that this phase is mechanical stable. However, its enthalpy is not the lowest one among all structures observed currently. Thus, the δ-$CHBr_3$ is a metastable phase at low temperature.

The ε phase has four molecules with polar symmetry in its unit cell. The calculated lattice parameters of this phase at 100 GPa are $a = 7.9221$ Å, $b = 4.77276$ Å, $c = 9.47399$ Å, and $\beta = 146.709°$, with atomic positions of H at 4*a* (0.53771, −0.57003, 0.56517), C at 4*a* (0.34586, −0.63987, 0.3730), and Br at 4*a* (0.12833, −0.85657, 0.34307), 4*a* (0.50305, −0.85643, 0.34256), and 4*a* (0.14517, −0.33068, 0.17216). The equation of state (EOS) of the ε phase, shown in Figure 5, is determined by fitting the pressure as a function of volume to the Murnaghan equation of state[31] $P = (B_0/B_0')[(V/V_0)^{B_0'} - 1]$, where $V_0$ is the equilibrium volume at zero pressure, $B_0$ is the bulk modulus at zero pressure, and $B_0'$ is the derivative of $B_0$ with respect to pressure. On the basis of these results, $V_0$, $B_0$, and $B_0'$ were calculated to be 218.56 ± 8.58 Å$^3$, 29.63 ± 4.48 GPa, and 3.08 ± 0.04, respectively.

The ε phase can be considered as a layered structure, all of the CH groups direct to one side of the layer that consists of bromine atoms and carbon atoms nearly. The neighboring layers in the ε phase are stacked in the alternating ABAB manner as shown in Figure 6c. In the δ phase, the polar molecules have the same orientation, with the H atoms pointing to the [001] axis (Figure 6b). In addition, the β and γ phases are made of molecular polar layers, but the consecutive layers are antiparallel, and the arrangement can be considered as comprising bilayers of bromine triangles parallel to the basal plane, with the C−H bond in the interior of the bilayer (see Figure 6a). The bilayers are defined as two layers of $CHBr_3$ molecules linked by C−H···Br hydrogen bonds.

The two main factors that determine the molecular association are the molecular structure and the noncovalent interactions between molecules, such as hydrogen bond and halogen bond.[32−34] In the case of bromoform, the C−H···Br and Br···Br attraction dominate the intermolecular interaction, which depends strongly on the intermolecular distances. For the ordered polar δ phase, only the C−H···Br contacts are shorter than

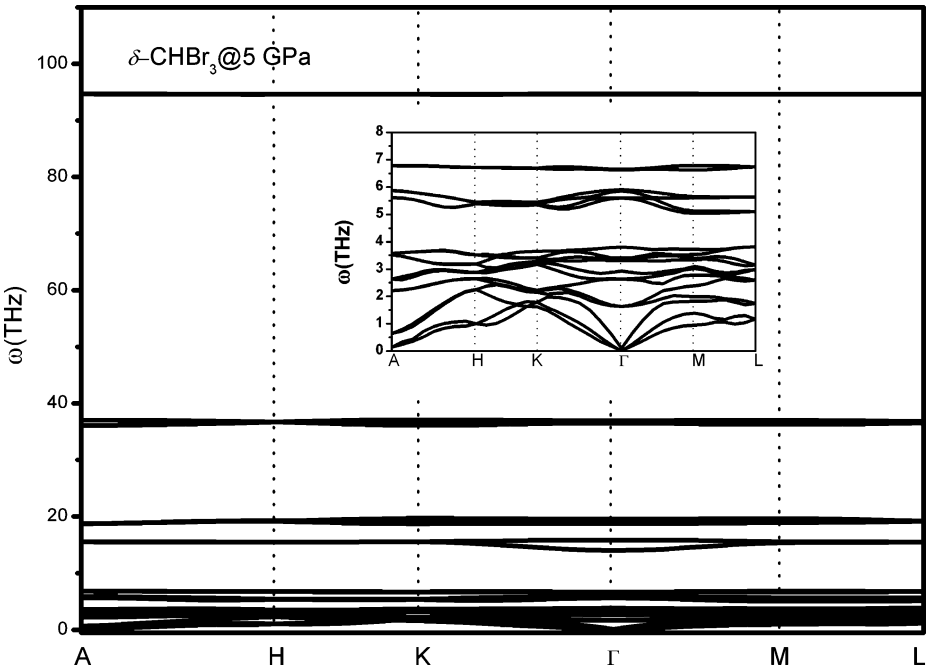


**Figure 4.** Calculated phonon dispersion curve of the δ phase at 5 GPa. Inset: the magnified frequency from 0 to 8 THz.

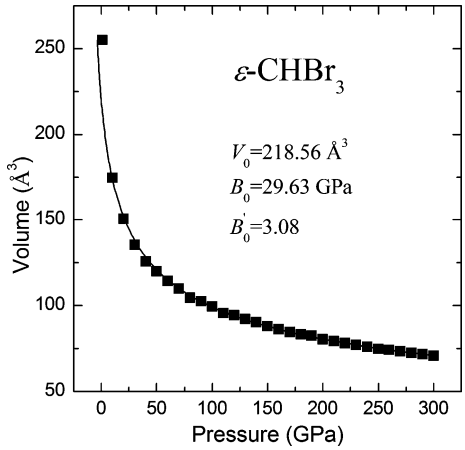


**Figure 5.** Equations of state for the $\varepsilon$ phase. Solid line through the calculated data points represents fitted curves using the Murnaghan equation of state.

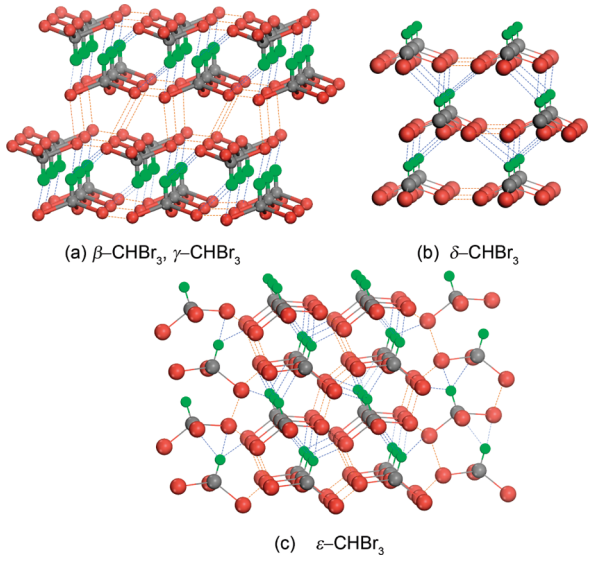


**Figure 6.** A perspective view of the *bc* plane shows the 3D-network molecular structure of $\beta$-$CHBr_3$, $\gamma$-$CHBr_3$, $\delta$-$CHBr_3$, and $\varepsilon$-$CHBr_3$ with the intermolecular hydrogen bonding and halogen bonding interactions. The blue and yellow dashed lines represent C−H···Br hydrogen bonds and Br···Br halogen bond, respectively.

the sums of van der Waals radii under its formation condition, as shown in Table 3. In the ordered centrosymmetric $\beta$ and $\gamma$ phases, only the intrabilayer C−H···Br have contacts shorter than van der Waals radii (Table 3) at ambient pressure. Owing to this, the interactions C−H···Br in the $\delta$, $\beta$, and $\gamma$ phases

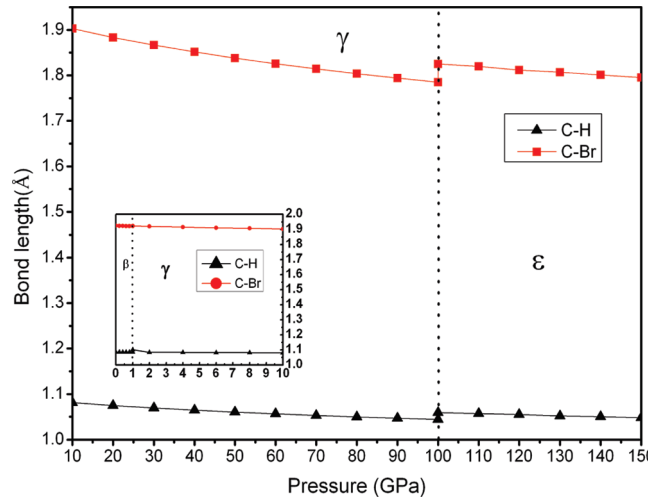


**Figure 7.** Pressure dependence of bond length C−H and C−Br. Inset: the magnified bond length from 0 to 10 GPa.

are more favorable than the Br···Br interactions. With an increase in pressure, the intrabilayer distances C−H···Br and intra- and interbilayer distances Br···Br gradually decrease (Table 3), indicating that two kinds of interactions intensify with pressure. The significant intermolecular interactions are capable of compensating the energy cost of the dipolar ordering within domains. In the $\varepsilon$ phase at about 100 GPa, the distances of C−H···Br and Br···Br are shorter than the sums of the van der Waals radii, and two kinds of interactions become stronger. Thus, these C−H···Br and Br···Br interactions between the neighboring layers are the key factors for the formation of the polar structure.

A complementary insight into the relation between high-pressure phase transition of bromoform and bond length change has been obtained. The changes in the C−H and C−Br bond lengths for the $\beta$, $\gamma$, and $\varepsilon$ phases in their corresponding existing pressures are shown in Figure 7. It was found that bond lengths of C−H and C−Br monotonically decrease within their exiting pressure range but have a discontinued change at the phase transition pressures. Unlike iodoform, the abnormal behavior of C−H bond with pressure was not found in bromoform, implying that the interactions C−H···I and C−H···Br characterize different properties.

The calculated energy band structures of $\beta$, $\gamma$, and $\varepsilon$ phases of $CHBr_3$ at selected pressure are shown in Figure 8. At ambient pressure, the $\beta$ phase has an indirect band gap of 3.55 eV, as illustrated in Figure 8a, which is an insulator. The bands are flat, indicating that the solid bromoform is a typical molecular

**TABLE 3: The Calculated Interlayer Br···Br and H(D)···Br Distances in the Bromoform Comparing with Experimental Data at Selected Pressures**

| | pressure GPa | structure | distance Br···Br, Å | distance H(D)···Br, Å |
|---|---|---|---|---|
| exptl | 0 | $\beta$-$CDBr_3$ (14 K)[10] | 3.968/4.052/4.102 (within one bilayer) 3.935/4.021/4.116 (between bilayers) | 2.909 |
| | | $\gamma$-$CDBr_3$ (14 K)[10] | 4.007 (within one bilayer) 4.075 (between bilayers) | 2.922 |
| | 0.35 | $\delta$-$CHBr_3$ (295 K)[13] | 3.724 | 3.053 |
| calcd | 10 | $\gamma$-$CHBr_3$ (0 K) | 3.493 (within one bilayer) 3.397 (between bilayers) | 2.556 |
| | 90 | $\gamma$-$CHBr_3$ (0 K) | 2.9238 (within one bilayer) 2.7683 (between bilayers) | 2.014 |
| | 100 | $\varepsilon$-$CHBr_3$ (0 K) | 2.578 (between layers) | 1.986 |

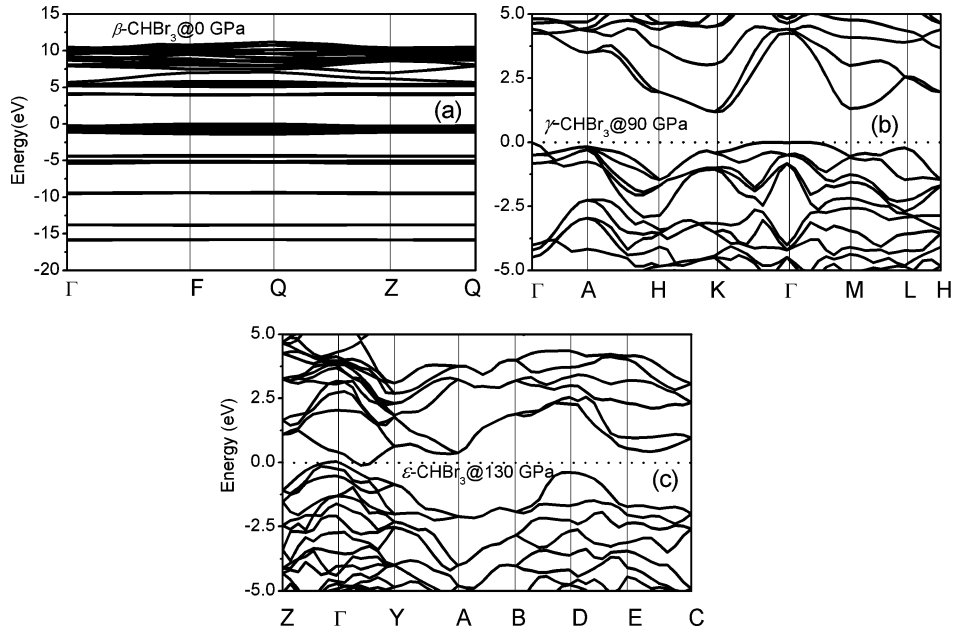


**Figure 8.** Energy band structures of solid $CHBr_3$: (a) $\beta$ phase at 0 GPa, (b) $\gamma$ phase at 90 GPa, and (c) $\varepsilon$ phase at 130 GPa.

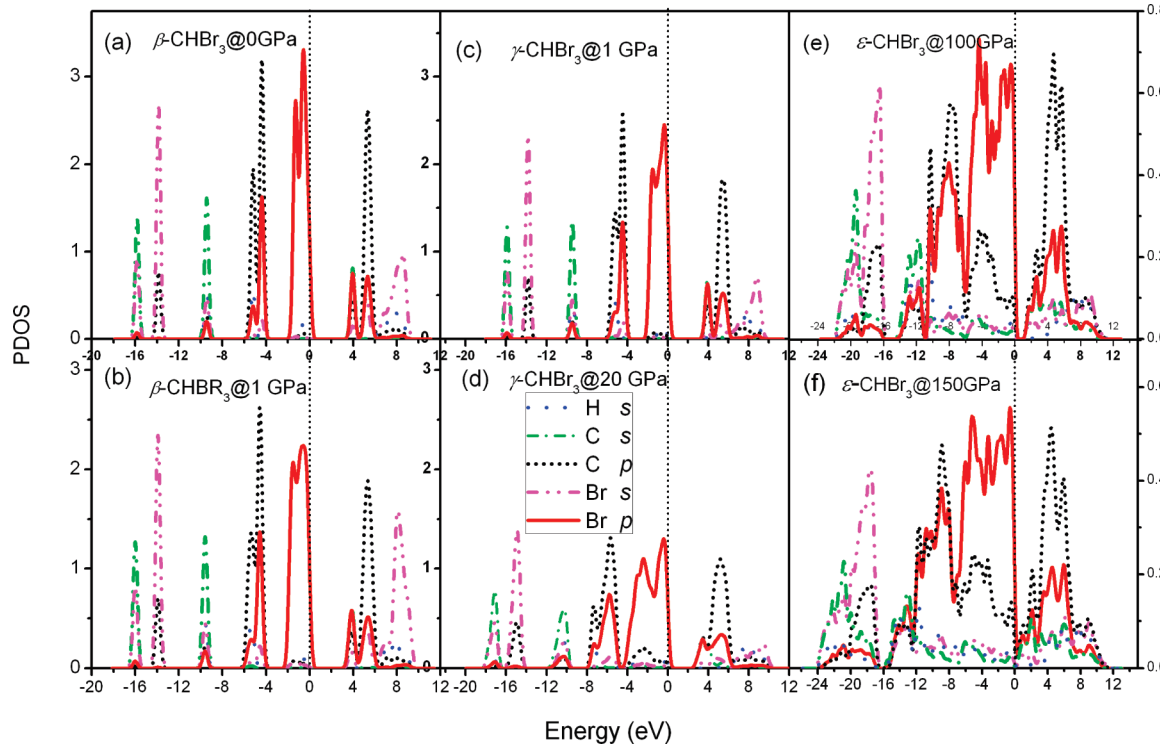


**Figure 9.** The calculated partial electronic density of states (PDOS) for Br, C, and H in $\beta$-$CHBr_3$, $\gamma$-$CHBr_3$, and $\varepsilon$-$CHBr_3$ phases at different pressures.

crystal. It is also characterized by the coexistence of strong intramolecular and weak intermolecular bondings, implying that the electrons strongly locate at the intramolecular space. The van der Waals force here is mainly the dispersion forces originated by the instant molecular dipole interactions.[35]

The PDOS of the $\beta$, $\gamma$, and $\varepsilon$ phases with increasing pressure are shown in Figure 9. The valence bands (VB) of $\beta$ phase at ambient pressure occur in five groups. The lowest band ($VB_1$) ($\sim$−16 eV) is contributed mainly by C 2s and Br 4s and slightly by H s. The second valence band ($VB_2$) ($\sim$−14 eV) is generated from Br 4s and C 2p. The third valence band ($VB_3$) ($\sim$−9.5 eV) comes mainly from H s and C 2s and slightly from Br 4s4p and C 2p. The fourth valence band ($VB_4$) ($\sim$−5.4 eV) is formed mainly by C 2p and Br 4p and slightly by H s. The highest valence band ($VB_5$) (0 $\sim$ −1.5 eV) is attributed to Br 4p. The first conducting bands of the $\beta$ phase at ambient pressure are dominated by Br 4p, C 2s, and C 2p, whereas the second conducting band comes mostly from C 2p, Br 4s, and Br 4p and a small protion from H s, as shown in Figure 9a.

From the calculated energy band structures, it is clearly seen that the $\gamma$-$CHBr_3$ exists as an insulator in the pressure range from 1 to 90 GPa (see Figure 8b), and the $\varepsilon$-$CHBr_3$ begins to metalize at 130 GPa (see Figure 8c). With the increase of pressure, the bands become more dispersive, the hybridization

among C s, p and Br s, p states increase. In the $\gamma$-$CHBr_3$, there is no evidence of metallization, implying the strong localization of electrons as well as the weaker attractive Br···Br interactions[36] due to the hybridization way of carbon atoms is $sp^3$, which also may be illustrated from the change of PDOS with pressure (Figure 9c and d). In the $\varepsilon$-$CHBr_3$ phase, Br-derived valence band steps up and Br and C-derived conducting band steps down first cross the Fermi level. Br−Br antibonding states located above the Fermi energy level are dominated by Br 4p ($\pi^*$ bonds) states. Above 130 GPa, the bands overlap, and the Fermi level is mainly dominated by Br p electrons, as shown in Figure 9e and f. On the other hand, it is very interesting that the strongest C−H stretching vibrations of $\varepsilon$-$CHBr_3$ observed around 100 THz in the high-energy region at 300 GPa exhibit an obvious molecular feature (Figure 3), although it has metalized at this pressure.

## Conclusion

In summary, theoretical calculations have revealed a novel monoclinic structure of bromoform at high pressure. This structure ($\varepsilon$ phase) exhibits a polar symmetry with space group *CC*. In addition, we have successfully mimicked the following phase transition sequence of bromoform at zero temperature: from $\beta$ phase to $\gamma$ phase at 1 GPa, then to $\varepsilon$ phase at 90 GPa, which is stable at least up to 300 GPa, the highest pressure studied. The pressure-induced metallization in the $\varepsilon$ phase happens at 130 GPa, and the metallic behavior mainly caused by the hybridization of C s, p and Br s, p. It has been demonstrated that the electrostatic contribution to Br···Br and C−H···Br interactions in the $\varepsilon$ phase are favorable for polar aggregation, and these effects intensify with increasing pressure.

**Acknowledgment.** We are thankful for financial support from the National Natural Science Foundation of China (No. 10979001), the National Basic Research Program of China (No. 2005CB724400), the Cheung Kong Scholars Program of China, Changjiang Scholar and Innovative Research Team in University (No. IRT0625) and the National Fund for Fostering Talents of Basic Science (No. J0730311).

## References and Notes

(1) Curtin, D. Y.; Paul, I. C. *Chem. Rev.* **1981**, *81*, 525–541.
(2) Zhang, H.; Wang, X. M.; Zhang, K. C.; Teo, B. K. *J. Solid State Chem.* **2000**, *152*, 191.
(3) Zerr, A.; Serghiou, G.; Boehler, R.; Ross, M. *High Pressure Res.* **2006**, *26*, 23–32.
(4) Zhao, J.; Feng, W. X.; Liu, Z. M.; Ma, Y. M.; He, Z.; Cui, T.; Zou, G. T. *Chin. Phys. Lett.* **2010**, *27*, 066101.
(5) Kenichi, T.; Kyoko, S.; Hiroshi, F.; Mitsuko, O. *Nature* **2003**, *423*, 971–974.
(6) Duan, D. F.; Liu, Y. H.; Ma, Y. M.; Liu, Z. M.; Cui, T.; Liu, B. B.; Zou, G. T. *Phys. Rev. B* **2007**, *76*, 104113.
(7) Zeng, Q. F.; He, Z.; San, X. J.; Ma, Y. M.; Tian, F. B.; Cui, T.; Liu, B. B.; Zou, G. T.; Mao, H. K. *Proc. Natl Acad. Sci. U.S.A.* **2008**, *105*, 4999–5001.
(8) Dziubek, F. K.; Katrusiak, A. *J. Phys. Chem. B* **2008**, *112*, 12001.
(9) Liu, D.; Lei, W. W.; Wang, K.; Bao, G.; Li, F. F.; Hao, J.; Liu, B. B.; Cui, T.; Cui, Q. L.; Zou, G. T. *J. Phys. Chem. B* **2009**, *113*, 7430.
(10) Myers, R.; Torrie, B. H.; Powell, B. M. *J. Chem. Phys.* **1983**, *79*, 1495.
(11) Shimizu, H.; Matsumoto, K. *J. Phys. Soc. Jpn.* **1984**, *53*, 4438.
(12) Zhao, Y.; Luo, H.; Lu, X.; Zou, G. *Phys. B+C* **1986**, *139−140*, 526–529.
(13) Kamil Dziubek, F.; Katrusiak, A. *J. Phys. Chem. B* **2008**, *112*, 12001.
(14) Coulson, C. A.; Emerson, D. *Proc. R. Soc. London, Ser. A* **1974**, *337*, 151.
(15) Hatch, D. M.; Stokes, H. T. *J. Phys.: Condens. Matter* **1990**, *2*, 1121.
(16) Burgos, E.; Halac, E. B. *Chem. Phys.* **1991**, *161*, 77.
(17) Stanila, D.; Smith, W.; Anderson, A. *Spectrosc. Lett.* **2001**, *34*, 199–210.
(18) Segall, M.; Lindan, P.; Probert, M.; Pickard, C.; Hasnip, P.; Clark, S.; Payne, M. *J. Phys.: Condens. Matter* **2002**, *14*, 2717.
(19) Vanderbilt, D. *Phys. Rev. B* **1990**, *41*, 7892.
(20) Pfrommer, B. G.; Côté, M.; Louie, S. G.; Cohen, M. L. Relaxation of Crystals with the Quasi-Newton Method. *J. Comput. Phys.* **1997**, *131*, 233–240.
(21) Perdew, J. P.; Burke, K.; Ernzerhof, M. *Phys. Rev. Lett.* **1996**, *77*, 3865.
(22) Monkhorst, H. J.; Pack, J. D. *Phys. Rev. B* **1976**, *13*, 5188.
(23) Rappe, A. K.; Casewit, C. J.; Colwell, K. S.; Goddard, W. A.; Skiff, W. M. *J. Am. Chem. Soc.* **1992**, *114*, 10024–10035.
(24) Parlinski, K. computer code PHONON, http://wolf.ifj.edu.pl/phonon.
(25) Giannozzi, P.; Baroni, S.; Bonini, N.; Calandra, M.; Car, R.; Cavazzoni, C.; Ceresoli, D.; Chiarotti, G. L.; Cococcioni, M.; Dabo, I.; Corso, A. D.; Gironcoli, S. d.; Fabris, S.; Fratesi, G.; Gebauer, R.; Gerstmann, U.; Gougoussis, C.; Kokalj, A.; Lazzeri, M.; Martin-Samos, L.; Marzari, N.; Mauri, F.; Mazzarello, R.; Paolini, S.; Pasquarello, A.; Paulatto, L.; Sbraccia, C.; Scandolo, S.; Sclauzero, G.; Seitsonen, A. P.; Smogunov, A.; Umari, P.; Wentzcovitch, R. M. *J. Phys.: Condens. Matter* **2009**, *21*, 395502.
(26) Mujica, A.; Rubio, A.; Muñoz, A.; Needs, R. J. *Rev. Mod. Phys.* **2003**, *75*, 863.
(27) Ma, Y.; Oganov, A. R.; Li, Z.; Xie, Y.; Kotakoski, J. *Phys. Rev. Lett.* **2009**, *102*, 065501.
(28) Andrews, B.; Anderson, A.; Torrie, B. H. *Chem. Phys. Lett.* **1983**, *101*, 392.
(29) Burgos, E.; Halace, E.; Bonadeo, H. *J. Chem. Phys.* **1981**, *74*, 1546.
(30) Wu, Zh. J.; Zhao, Er. J.; Xiang, H. P.; Hao, X. F.; Liu, X. J.; Meng, J. *Phys. Rev. B* **2007**, *76*, 04115.
(31) Murnaghan, F. *Proc. Natl Acad. Sci. U.S.A.* **1944**, *30*, 244.
(32) Wang, K.; Duan, D.; Wang, R.; Liu, D.; Tang, L.; Cui, T.; Liu, B.; Cui, Q.; Liu, J.; Zou, B.; Zou, G. *J. Phys. Chem. B* **2009**, *113*, 14719–14724.
(33) Wang, L. C.; Tian, F. B.; Feng, W. X.; Chen, C. B.; He, Z.; Ma, Y. M.; Cui, T.; Liu, B. B.; Zou, G. T. *J. Chem. Phys.* **2010**, *132*, 164506.
(34) Berski, S.; Ciunik, Z.; Drabent, K.; Latajka, Z.; Panek, J. *J. Phys. Chem. B* **2004**, *108*, 12327–12332.
(35) Kawaguchi, T.; Takashina, K.; Tanaka, T.; Watanabe, T. *Acta Crystallogr.* **1972**, *B28*, 967.
(36) Awwadi, F. F.; Willett, R. D.; Peterson, K. A.; Twamley, B. *Chem.—Eur. J.* **2006**, *12*, 8952.

JP103823C